

SKB P-25-06

ISSN 1651-4416

ID 2084130

September 2025

Homogenisation of bentonite in long steel tubes

Two tests completed after eleven years

Ann Dueck, Ola Kristensson, Viktor Jensen
Clay Technology Lund AB

Keywords: Bentonite, Swelling, Swelling pressure, Homogenisation, Long-time analysis

This report concerns a study which was conducted for Svensk Kärnbränslehantering AB (SKB). The conclusions and viewpoints presented in the report are those of the authors. SKB may draw modified conclusions, based on additional literature sources and/or expert opinions.

Data in SKB's database can be changed for different reasons. Minor changes in SKB's database will not necessarily result in a revised report. Data revisions may also be presented as supplements, available at www.skb.se.

This report is published on www.skb.se

© 2025 Svensk Kärnbränslehantering AB

Abstract

Homogenisation properties of bentonite are studied with long-time homogenisation tests in steel tubes. Initially, ten tests of this type were started, and MX-80 was used for all specimens. The results of two of the specimens, dismantled after 11 years, have been reported here. The results have been presented in terms of dry density distributions and stress measurements.

The long-term perspective of the homogenisation process in the tests was studied using two different approaches. In a direct approach, a homogenisation indicator was formulated using statistical properties of the dry density distribution. An indirect approach, used in a previous study, is based on an analytical solution of a mechanical model which includes friction between the buffer and the tube inner surface. The outcome from this is an estimate of a friction angle.

The findings from the direct approach are e.g. that the homogenisation has progressed with time between all terminated tests and that the rate of progression decreases with time. The findings from the indirect approach also agrees well with this and the computed friction angles agree well with values computed in earlier analyses.

Sammanfattning

Homogeniseringsegenskaperna hos bentonit har studerats med långtidshomogeniseringstester i stålrör. Inledningsvis påbörjades tio stycken tester av denna typ, och MX-80 användes för alla prover. Resultaten av två av proverna, som demonterades efter 11 år, har rapporterats här. Resultaten har presenterats som fördelning av torrdensitet och spänningsmätningar.

Det långsiktiga perspektivet på homogeniseringsprocessen i testerna studerades med hjälp av två olika tillvägagångssätt. I ett direkt tillvägagångssätt formulerades en homogeniseringsindikator med hjälp av statistiska egenskaper hos torrdensitetsfördelningen. En indirekt ansats, som använts tidigare i projektet, bygger på en analytisk lösning av en mekanisk modell som inkluderar friktion mellan bufferten och rörets inre yta. Resultatet av detta är en uppskattning av en friktionsvinkel.

Resultaten från den direkta metoden är t.ex. att homogeniseringen har fortskridit med tiden mellan alla avslutade tester och att hastigheten i fortskridandet minskar med tiden. Resultaten från den indirekta ansatsen stämmer också väl överens med detta och de beräknade friktionsvinklarna stämmer väl överens med de värden som beräknats i tidigare analyser.

Content

1	Introduction	3
1.1	Objectives	3
1.2	Material	3
2	Determinations of water content and density	4
3	Description of the experiment	5
3.1	Test setup	5
3.2	Test procedure	7
4	Sensor and dismantling data for tests FLR3 and FLR8	8
4.1	Stress measurements	8
4.2	Termination, dismantling and sampling	10
4.3	Distribution of water content and density	10
4.4	Comments	12
5	Investigation of the homogenisation process	16
5.1	Direct approach – statistical method	16
5.1.1	Disagreement between data reported at installation and dismantling	17
5.2	Indirect approach – analytical mechanical representation	19
6	Concluding remarks	21
	References	22
	Appendix 1	23

1 Introduction

The study presented here is a part of an SKB research topic where the self-sealing and homogenisation properties of bentonite are studied. The laboratory part consists of different types of tests, e.g. fundamental swelling tests, measurement of friction between bentonite and other surfaces, homogenisation after loss of bentonite and homogenisation in long tubes.

An important part of this homogenisation study consists of long-time homogenisation tests in steel tubes. The purpose of these tests is to study the effect of friction for limiting homogenisation and also to study the change in density gradients with time after completed swelling and compression. The results can also be utilised to evaluate to what extent the so called “transition zones” in tunnels can be used to downshift the swelling pressure against e.g. a plug.

Ten individual tests were initially included in the experiment. By using different test durations before termination and sampling, long-term effects on the distribution of density can be studied. The results from two tests, FLR3 and FLR8, which ended after eleven years, are analysed in this report. As reported by Dueck et al. (2018, 2022), three tests have previously been completed, FLR5 after 2 years, FLR6 after 4 years, and FLR7 after 6 years. Of the initially installed ten tests, five are still ongoing.

The results from the previously terminated tests were analysed by using an analytical model based on force equilibrium after pore pressure equilibrium. The force equilibrium included the friction between the bentonite and the side walls. A friction angle was evaluated from the measured length of the transition zone and the measured stresses. See Dueck and Börjesson (2021) and Dueck et al. (2019).

1.1 Objectives

One objective with this report is to present results from the two tests, FLR3 and FLR8, terminated after 11 years in June 2024. The results presented are stresses measured during the test period and distributions of water content and dry density. The new data is also compared to what was obtained for the previously completed tests.

Another objective is to evaluate the progression of homogenisation in the dry density distribution. Here, an approach, novel for this study, using the standard deviation of the distribution, is described and utilised. Comparisons of evaluated friction angles are also related to this objective.

1.2 Material

The bentonite materials used is the commercial sodium dominated Wyoming bentonite with brand name Volclay MX-80 from American Coll. Co. Descriptions of the materials and basic variables were presented by e.g. Svensson et al. (2011).

The bentonite powder (CT 2012) was delivered with an approximate water content of 10%. Since higher initial water content was needed for the tests, the powder was mixed with de-ionized water. Placed in a mould, the powder was then compacted to a block in a hydraulic press. The bentonite pellet (CT 2011) was used as delivered, some individual pellets, however, were split to get the predetermined mass into the equipment.

2 Determinations of water content and density

The basic variables water content and bulk density are determined after dismantling of each test and from these variables the dry density and degree of saturation are calculated. The water content is usually determined on one half of the dismantled specimen and the bulk density on the other half. The water content w (%), void ratio e (-), degree of saturation S_r (%), and dry density ρ_d (kg/m³), are calculated using Equations 2-1 to 2-4, with the particle density $\rho_s = 2780$ kg/m³ and the water density $\rho_w = 1000$ kg/m³ (see e.g. Karnland et al., 2006).

$$w = 100 \frac{m_{tot} - m_s}{m_s} \quad (2-1)$$

$$e = \frac{\rho_s}{\rho} (1 + w/100) - 1 \quad (2-2)$$

$$S_r = \frac{\rho_s \cdot w}{\rho_w \cdot e} \quad (2-3)$$

$$\rho_d = \frac{m_s}{V} \quad (2-4)$$

where

m_{tot} = total mass of a sample

m_s = dry mass of a sample

V = total volume of a sample

ρ_s = particle density

ρ_w = density of water

ρ = bulk density of a sample

The dry mass is obtained from measuring the weight after drying a wet sample at 105 °C for 24h. The bulk density is calculated from the total mass of a sample and the volume determined by measuring the weight when the sample is suspended in air and when it is submerged in paraffin oil. With the density of paraffin oil known, the volume of the sample can be calculated.

3 Description of the experiment

A comprehensive description of the tests and results have previously been presented by Dueck et al. (2018, 2022). The short description below is provided as a recapitulation of the main features of the experiment for better understanding of the tests results.

3.1 Test setup

A general sketch of the setup used in this series is shown in Figure 3-1. The height of the tubes is ten times the diameter and the tubes are placed in an upright position during the tests. The lower half of the tubes was filled with highly compacted bentonite and the upper half was filled with bentonite pellets. The material used in this test type is MX-80.

Four different varieties of the tubes were manufactured with the main difference being the vertical profile of the inner surface and the dimensions of the tubes, Figure 3-2. For all but one test (FLR3), the inner surface had a non-smooth profile consisting of machined horizontal grooves to increase the friction between the bentonite and the tube. The type of profile is indicated with different lines in Figure 3-2; rectangular shaped grooves (grey lines), triangular shaped grooves (black lines) and a smooth inner wall (no lines). Two different dimensions of tubes were used, nine had the inner diameter 25 mm (and height 250 mm), and one (FLR4) had the inner diameter 35 mm (and height 350 mm).

For tests FLR1-FLR4, force transducers measured axial and radial force as indicated in Figure 3-1. The force was transferred from the buffer to the transducer via a piston which, knowing the piston area, enabled calculation of the corresponding total stress. The tests FLR1 to FLR4 were run according to Figure 3-2 while tests FLR5 - FLR10 were run with similar conditions as FLR2 but without any measurements of total stress. The grooves of the inner surface of the steel tubes are shown in Figure 3-3.

Details about each specimen used in tests FLR1 to FLR10, including the initial target dry density, are shown in Table 3-1.

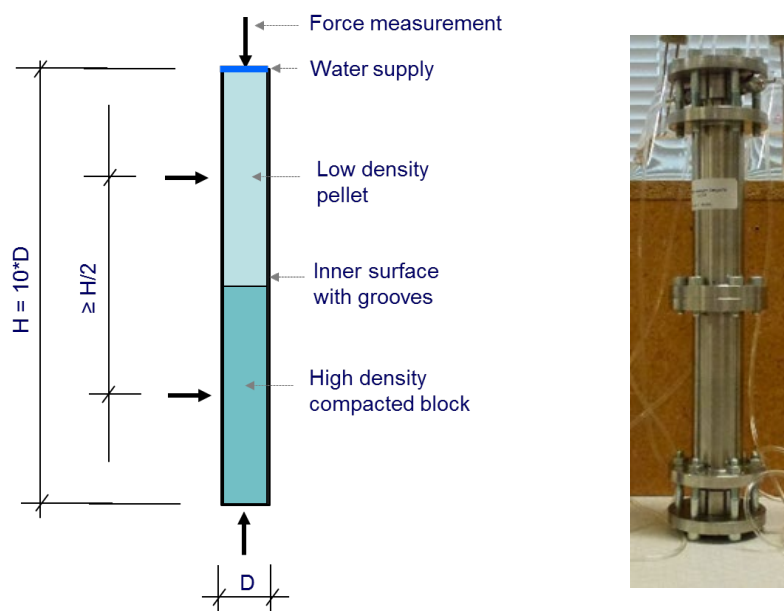


Figure 3-1. Sketch and photo of the Long Steel Tubes used in the test series. Axial and radial stress measurements are made in some of the tubes (marked with arrows).

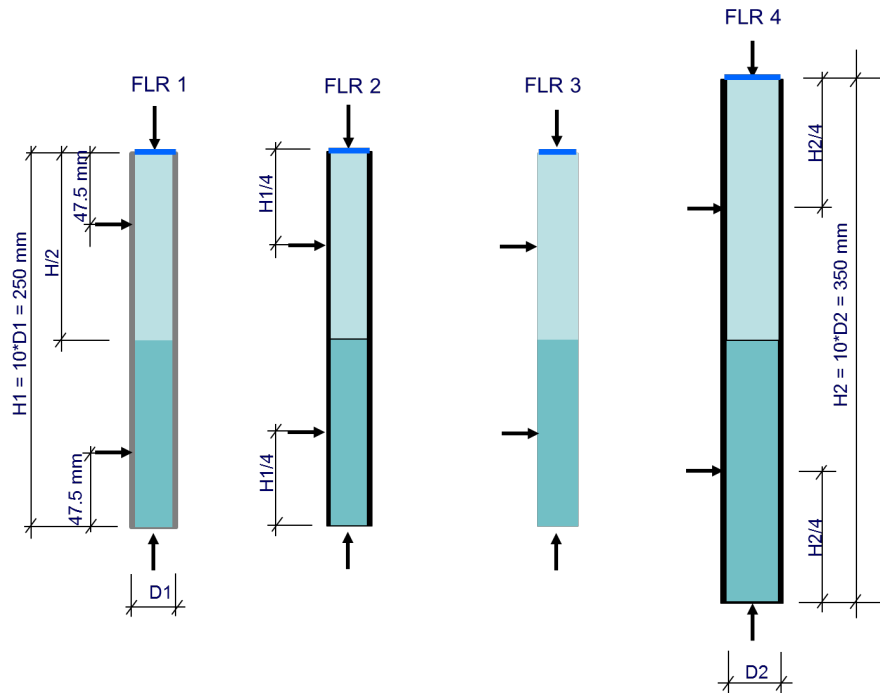


Figure 3-2. Sketches of the tubes used in the test series and the boundary conditions of tests FLR1 to FLR4. The different lines surrounding the specimens denote the different features of the inner surface of the tubes (grey line = rectangular grooves, black line = triangular grooves, no line = polished smooth surface). The tests FLR5 - FLR10 were run in tubes similar to the one used for test FLR2 but without total stress measurements.

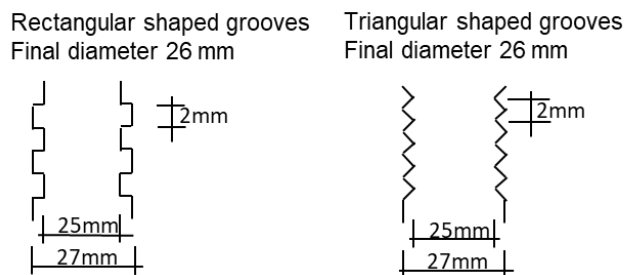


Figure 3-3. Grooves of the inner surfaces of FLR1 (rectangular) and FLR2, FLR4, FLR5-FLR10 (triangular).

Table 3-1. Test conditions and target initial densities for all specimens in the series with long tubes. The initial target densities were calculated from the mass and the final volume

Labels	FLR1	FLR2	FLR3	FLR4	FLR5 - FLR10
Start date	March 2012	May 2013	May 2013	May 2013	May 2013
Setup					
Total height (mm)	250	250	250	350	250
Final average diameter (mm)	26	26	25	36	26
Inside friction (grooves)	rectangular	triangular	smooth	triangular	triangular
Stress measurements	yes	yes	yes	yes	no
Material upper half	MX-80 extruded pellet				
Material lower half	MX-80 high density blocks				
Water supply	From the upper drainage only				
Type of water	2-50 mM NaCl				
Initial target dry density					
Upper part ρ_d ,upper (kg/m3)	772	882	882	882	882
Lower part ρ_d ,lower (kg/m ³)	1566	1561	1561	1561	1561

3.2 Test procedure

The compacted material in the lower part of each tube consisted of 5 pre-compacted cylinder-shaped blocks placed on top of each other. The blocks had a height and diameter of 25 mm and 24.9 mm, respectively, or, in case of FLR4, a height of 35 mm and a diameter of 34.5 mm. The upper part with pellets was prepared by dividing each pellet into two pieces and putting them in place by hand to achieve the target dry density. After closing the tubes with pistons in both ends, load cells were attached to the instrumented tubes.

After air evacuation of filters, tubes and devices at test start, the devices were connected to a 2 mM NaCl-solution and initially open volumes, around pellets and between blocks and tube inner surfaces, were filled with water. Thus, the degree of saturation of the bentonite was approximately 100 % soon after test start.

In April/May 2014 the NaCl-concentration was increased to 50 mM NaCl in all tests, i.e. after two years for FLR1 and after one year for all other tests. In October 2015 a constant water pressure of 70 kPa was introduced for all devices except FLR1 and FLR5. However, already in September 2015 a water pressure between 0 and 100 kPa was applied for shorter intervals. For FLR1, a constant water pressure of 70 kPa was only introduced in January 2016, and FLR5 only had water supplied under atmospheric conditions during its testing time.

To be able to study the time effect on the density gradient, different testing times were planned for the ten tubes. At the time writing this report, tests have been dismantled after 2, 4, 6 and 11 years. The tests reported here, FLR8 and FLR3, were dismantled after 11 years. The date of the dismantling of the last tube has not yet been decided.

4 Sensor and dismantling data for tests FLR3 and FLR8

Below, the results from the two most recent dismantled tests, FLR3 and FLR8, are presented. They were dismantled after 11 years in an operation in June 2024. Stresses measured in FLR3 are shown together with stresses measured on FLR2, which resembles the dismantled but not instrumented FLR8. The process at termination, dismantling and sampling are described. Thereafter follows a presentation of the results in terms of distributions of water content and dry density. The new results are compared with previously dismantled tests in the series. Additional information is given in Appendix 1.

4.1 Stress measurements

In this section, total stresses measured in FLR3 are shown together with total stresses measured in FLR2, which resembles the dismantled but not instrumented FLR8. The evolution of total stress during the first eleven years, measured in FLR2, is shown in Figure 4-1 and the time for the dismantling of FLR5-FLR8 are marked (i.e. 2, 4, 6 and 11 years). The total stress evolution of FLR3, the only test with smooth inner surface, is shown in Figure 4-2.

Stresses at the time of dismantling FLR3 and FLR8, i.e. after 11 years, are tabulated in Table 4-1. The stresses are evaluated as average for 1.5 days. Before dismantling, the water pressure was lowered to zero, approximately 5-10 days before dismantling. This was also done before the dismantling of FLR8 and FLR3. Thus, the stresses of FLR3 in Table 4-1 was evaluated when the water pressure was zero.

The reduction of water pressure from 70 kPa to zero in FLR3 affected the total stress measured axially on the pellet side, i.e. at the position where the previous water pressure was applied, see Figure 3-1. The stress was reduced approximately 70 kPa. The total stress measured at the other three positions of FLR3 was, however, not significantly affected by the reduction of the water pressure. This finding is used throughout the analysis when evaluating the total stress measurements.

To be clear about the term swelling pressure, p_s , which will be used in the following, it usually denotes the total pressure, p , minus the water pore pressure, u , i.e. $p_s = p - u$. The total pressure is, in the present axisymmetric setup, given by $p = (\sigma_a + 2\sigma_r)/3$. However, since only one component, σ_a or σ_r , is known at a point, it is assumed that the unknown component is equal to the known, $\sigma_r = \sigma_a$ or $\sigma_a = \sigma_r$, respectively. Using that water pressure didn't affect the stress measurements significantly and the assumption of the unknown stress component gives that here, $p_s = \sigma_a$ or $p_s = \sigma_r$.

The evolution of the total stress from all four setups from start to June 2024 are shown in Appendix 1. Further comments on the evolution of the total stress are given in the Comments section below.

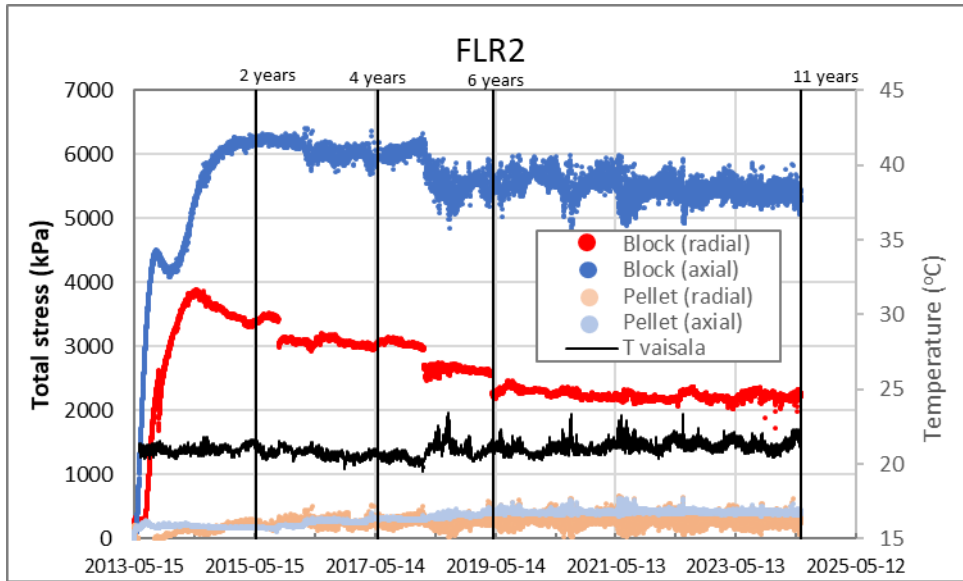


Figure 4-1. Evolution of total stress with time as total stress from start to 2024-06-07 with the time for the dismantling of FLR5, FLR6, FLR7, FLR8 after 2, 4, 6 and 11 years, respectively, are marked. The stresses were not measured on the dismantled setup but on the equivalent setup FLR2.

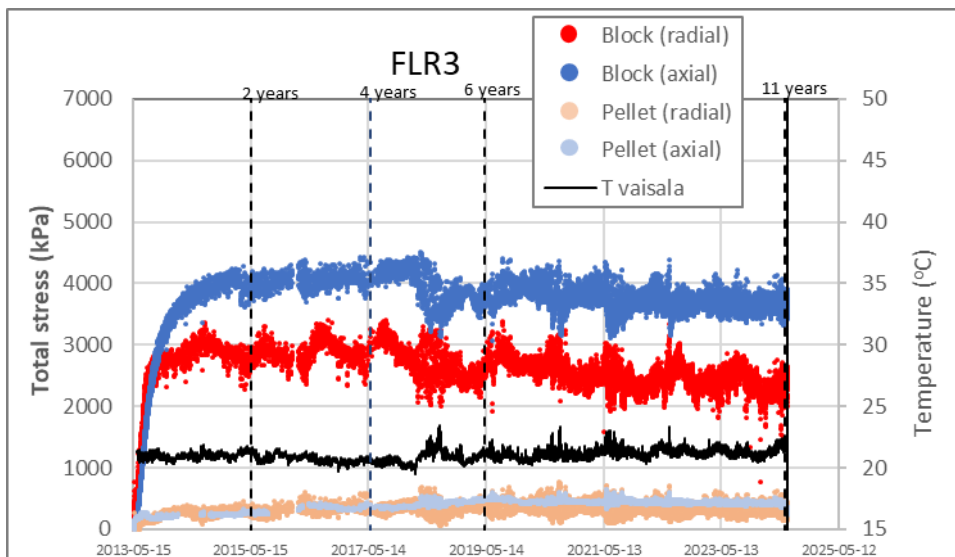


Figure 4-2. Evolution of total stress with time from FLR3 as total stress from start to 2024-06-27. The setup FLR3 was the only one with smooth inner surface and the dismantling of FLR3 after 11 years is marked (solid line). The time for the dismantling of other tests similar to setup FLR2 are also marked (dashed lines), see Figure 4-1.

Table 4-1. Total pressure, from setup FLR2 with similar setup as FLR8 and FLR3 at the time corresponding to the dismantling of FLR8 and FLR3, i.e. after 11 years

Distance ¹	Pellet or block ²	Total pressure 11 years (FLR8/FLR2)	Total pressure ⁴ 11 years (FLR3)	Direction ³
mm		kPa	kPa	
250	pellet	402	412 ⁴	axial
187.5	pellet	266	255	radial
62.5	block	2265	2249	radial
0	block	5296	5430	axial

¹ Distance from the bottom. ² Initial buffer type. ³ The total pressure is measured as the total radial and axial stresses. ⁴ The stresses were evaluated after lowering the water pressure to zero, which only affected the axially measured stress on the pellet side, see above.

For comparison, the corresponding values measured with the setup FLR1 after 11 years differed 6-30 % from the values measured with the setup FLR2 (given in Table 4-1). The measured stresses from FLR1 are given in Appendix 1. The setup FRL1 and FLR2 differ in that the positions of the radially measured stresses were slightly different (in the setup FLR1 the radially measurements were made at 47.5 mm and 202.5 mm from the bottom but 62.5 mm and 187.5 mm in the setup FLR2). In addition, different shapes of the grooves were used and while rectangular shaped grooves were used in FLR1 triangular ones were used in FLR2.

4.2 Termination, dismantling and sampling

The tests FLR8 and FLR3 were terminated on 2024-06-07 and 2024-06-27, respectively. The filters at the upper pistons and the connecting water supply tubes were emptied from fluid by a peristaltic pump and the samples were forced upwards through the steel tube. Samples with a thickness of 5-10 mm were taken continuously.

The sampling was made to provide information regarding:

- if the buffer and pellet sections were saturated,
- the dry densities at the positions of the pressure measurements,
- the distribution of dry density over the 250 mm specimen, with high resolution.

The degree of saturation was only determined for a few samples from the middle and from the lower part of the buffer. Determination of dry density were made for all samples by determining water content and assuming full saturation. See chapter 2 for more information about how the basic variables were obtained. The results for the two tests are given in the next section 4.3.

At dismantling of setup FLR3, the upper filter was stuck and larger load than expected was required to push the specimens out from below. The consequence of this was that the solid rod which was used to push the specimen out of the steel tube was pushed into the lower part of the specimen and material from this lower part was pushed out in the narrow gap between the rod and the steel tube. Approximately 38 mm of the lower part of the specimen was in this way influenced. The upper part is assumed not to have been affected. The lower part of FLR8 was also slightly affected, however only the lower 6 mm.

4.3 Distribution of water content and density

Both water content and density were determined on five (FLR8) or four (FLR3) samples. The results are presented in Table 4-2 and Table 4-3. The evaluated degree of saturations indicate that the buffer was fully saturated in both tests.

Table 4-2. Results from five samples from FLR8. The distances from the bottom to the centre of each sample are given with the thickness, water content, bulk density, dry density and the evaluated degree of saturation

Sample ID	Distance ¹ mm	Thickness mm	Water content %	Bulk density kg/m ³	Dry density kg/m ³	Degree of saturation %
FLR8-12	184	11.1	60.0	1680	1050	101
FLR8-18	145	12.1	54.0	1727	1121	102
FLR8-40	63	10.1	37.2	1883	1372	101
FLR8-46	27	10.1	33.5	1932	1447	101
FLR8-48	12	10.1	31.9	1960	1486	102

¹ Distance from the bottom.

Table 4-3. Results from four samples from FLR3. The distances from the bottom to the centre of each sample are given with the thickness, water content, bulk density, dry density and the evaluated degree of saturation

Sample ID	Distance ¹ mm	Thickness mm	Water content %	Bulk density kg/m ³	Dry density kg/m ³	Degree of saturation %
FLR3-12	186	10.1	61.0	1671	1038	101
FLR3-18	150	10.1	54.2	1718	1114	101
FLR3-29	89	10.1	39.2	1859	1335	101
FLR3-37	42	10.1	34.0	1922	1434	101

¹ Distance from the bottom.

The axial distributions of water content and dry density of the tests are shown in Figure 4-3. In the diagram to the right, circles mark the values from the samples where both water content and density were measured, cf. at the positions given in Table 4-2 and Table 4-3. The main part of the dry densities used in the diagram to the right was evaluated from the measured water contents and an assumption that the degree of saturation was 100 %. In the diagram to the right the initial target distribution of dry density is indicated by the dashed line. The initial target dry density in the lower part also includes radial swelling to the average radius of the inner surface profile. All values are tabulated in Appendix 1.

No large differences can be seen between the two density distributions obtained after 11 years. This is somewhat surprising since the inner surface of FLR3 was smooth while the inner surface of FLR8 had triangular grooves with a depth of 2 mm.

Due to the problems during the dismantling, described in section 4.2, there are uncertainties regarding the lower 38 mm in FLR3 and the lower 6 mm in FLR8. The uncertain values are marked with * in Figure 4-3.

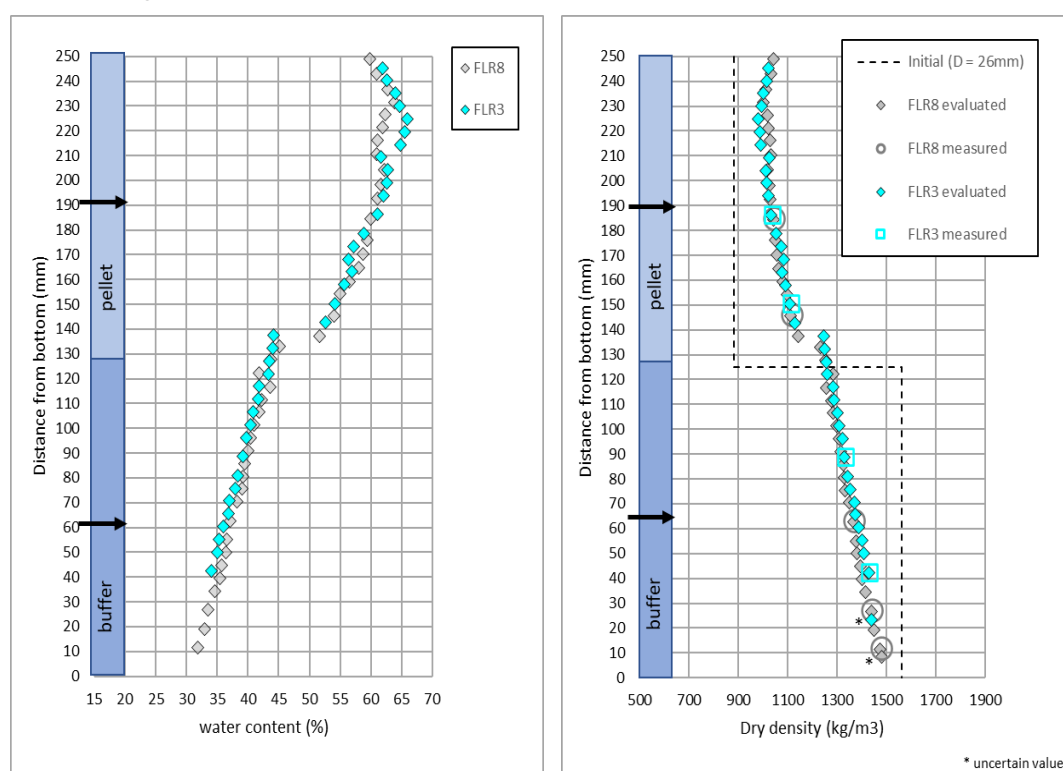


Figure 4-3. Distribution of water content (to the left) and dry density (to the right) after dismantling of FLR3 and FLR8. To the right the initial distribution of dry density, calculated with the final volume, i.e. final diameter, is also shown. The final dry density was determined from the water content and an assumption of $S_r = 100\%$ (labelled evaluated) and from measured water content and bulk density (labelled measured). The lower 38 mm of FLR3 and 6 mm of FLR8 are uncertain, see above.

4.4 Comments

In Figure 4-4 the results from Figure 4-3 are shown again together with the results from the previous dismantled specimens FLR5, FLR6 and FLR7 (Dueck et al., 2018, 2022). All densities given are calculated from measured water contents and assuming the degree of saturation 100 %, which is supported by the data in Table 4-2 and Table 4-3.

After dismantling the average dry density was evaluated according to Table 4-4 where the corresponding initial values are also given. From the table it can be seen that the average dry density of FLR5, FLR6 and FLR7 were higher than the average dry density of FLR3 and FLR8, which was caused by a slightly different height of the specimens. In Figure 4-5 the dry density ρ_d are therefore normalized with the ratio of the weighted actual average density $\rho_{d,FLRn}$ to the average dry density $\rho_{d,avr}$ of all three tests, according to Equations 4-1 to 4-4. The average density $\rho_{d,avr}$ was calculated to be 1241 kg/m³.

$$\rho_{d,normalized} = r_{FLRn} \rho_d \quad (4-1)$$

$$r_{FLRn} = \frac{\rho_{d,FLRn}}{\rho_{d,avr}} \quad (4-2)$$

$$\rho_{d,FLRn} = \frac{\sum(\rho_d \Delta h)}{\sum \Delta h} \quad (4-3)$$

$$\rho_{d,avr} = (\rho_{d,FLR3} + \rho_{d,FLR5} + \rho_{d,FLR6} + \rho_{d,FLR7} + \rho_{d,FLR8})/5 \quad (4-4)$$

Table 4-4. Results from FLR3 and FLR8 together with results from FLR5-FLR7 dismantled previously. The total time are given together with values of average dry density

Labels	FLR5	FLR6	FLR7	FLR8	FLR3
Start date	2013-05-15	2013-05-16	2013-05-16	2013-05-17	2013-05-22
End of test	2015-05-20	2017-05-29	2019-05-02	2024-06-07	2024-06-27
Total time	2 years	4 years	6 years	11 years	11 years
Initial target dry density					
Upper part $\rho_{d,upper}$ (kg/m ³)	882	882	882	882	882
Lower part $\rho_{d,lower}$ (kg/m ³)	1561	1561	1561	1561	1561
Average ρ_d (kg/m ³) ¹	1208	1211	1210	1210	1215
Final average dry density					
Upper part $\rho_{d,upper}$ (kg/m ³)	1067	1066	1070	1050	1040
Lower part $\rho_{d,lower}$ (kg/m ³)	1472	1438	1414	1359	1363
Average ρ_d (kg/m ³)	1270	1252	1243	1216	1223

¹The difference in initial average dry density was caused by slightly different total height of the specimens.

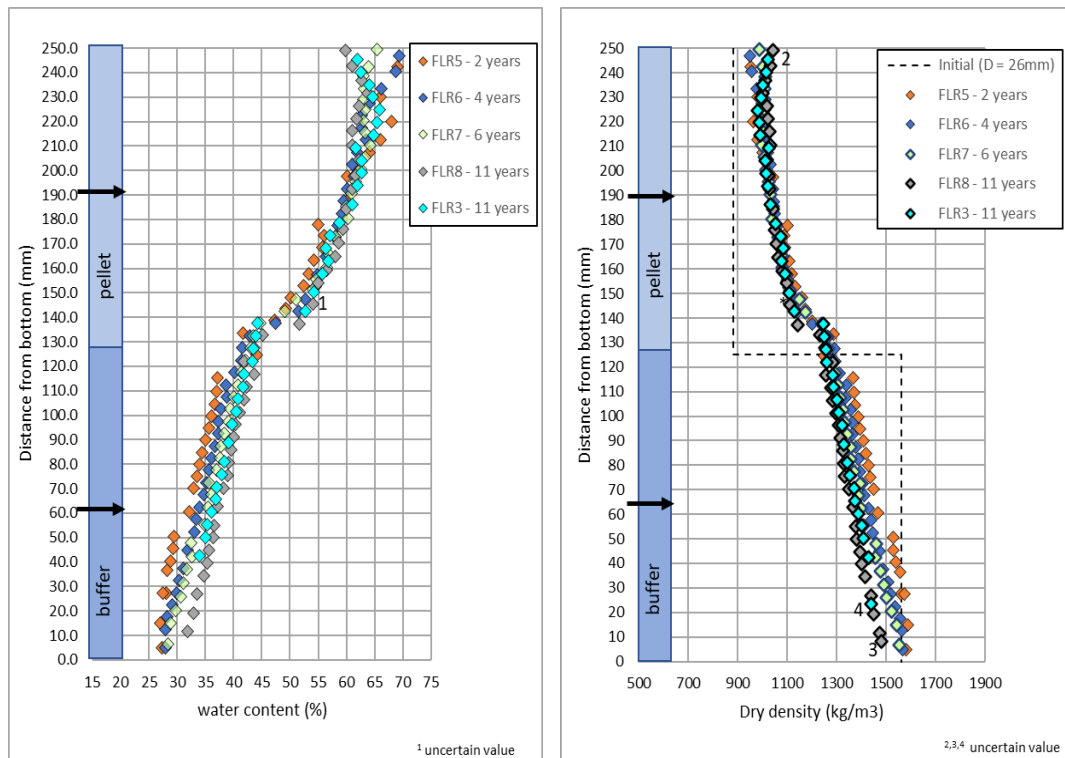


Figure 4-4. Distribution of dry density of FLR3 and FLR8 (from Figure 4-3) together with FLR5, FLR6 and FLR7 (Dueck et al., 2018, 2022). The dry densities were determined from the water content and $S_r = 100\%$. Notes 1-4 means: 1 - FLR6 uncertain water content, 2 - FLR7 uncertain position 243-250 mm, 3 - FLR8 uncertain position 0-6 mm, 4 - FLR3 uncertain position 0 - 38 mm.

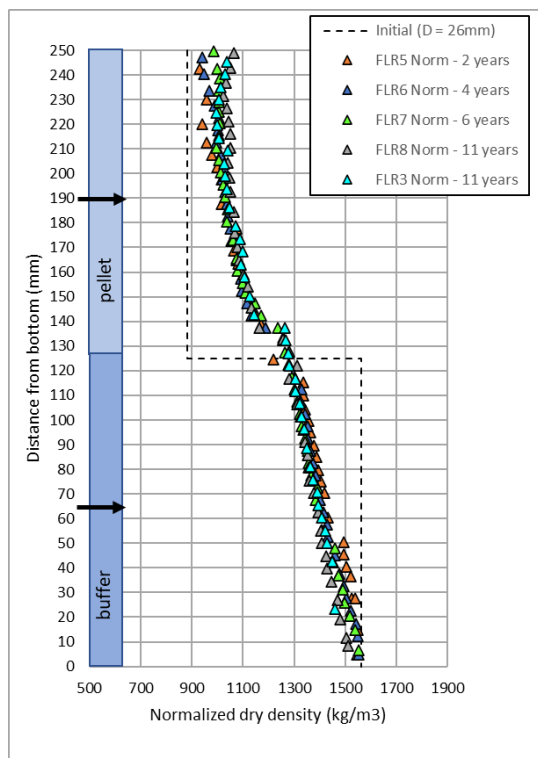


Figure 4-5. Distribution of normalized dry density where the dry density in Figure 4-4 are normalized with the ratio of the actual average density to the average dry density over all five specimens (i.e. 1241 kg/m^3).

A small change in the density distribution with time is indicated in Figure 4-5. In the lower part (0-50 mm) the density has decreased with time and the density at the bottom is less than the initial value (1561 kg/m³) in both FLR3 and FLR8, however, the values are somewhat uncertain from both these tests and no firm conclusion can be drawn. In the upper part (210-250 mm) a deviation from the initial value (882 kg/m³) was seen at all positions already after 2 years and an increase in dry density with time is indicated however with small differences over the height. Very small differences are seen in the density gradient between 50 and 210 mm but the initial step in density at mid-height seems to have moved upwards.

In Figure 4-6 the swelling pressure, here approximated by the total stress measurements σ_a or σ_r , is plotted as a function of the dry density after different times. Each dry density was measured, or interpolated between two measurements, at the specific position where the actual stress was measured. The results are also tabulated in Table 4-5 and Table 4-6. To the left in Figure 4-6 the dry densities measured after dismantling of FLR5, FLR6, FLR7 and FLR8 are plotted with the swelling pressure measured on the similar setup FLR2 at the actual time. While the measurements after 2, 4, and 6 years involved changes in both stress and dry density, the difference between 6 and 11 years is mainly a small change in dry density (a decrease in the lower block part of 30-60 kg/m³ (high stresses) and an increase in the upper pellet of 0-40 kg/m³ (at low stresses)). To the right in Figure 4-6 the results of FLR3 are shown, i.e. measured stresses as a function of dry density. In both diagrams the measurements after 11 years are close to one of the reference lines (dashed line).

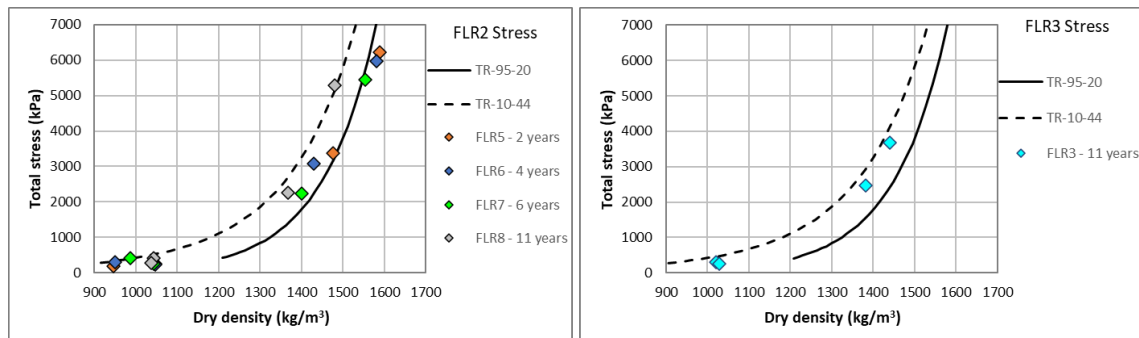


Figure 4-6. Total pressure as a function of dry density. Results after dismantling of FLR5, FLR6, FLR7 and FLR8 (after 2, 4, 6 and 11 years) plotted with total pressure measured on the similar setup FLR2 (to the left). Results after dismantling of FLR3 (to the right) after 11 years. Models presented by Börgesson et al. (1995) and Åkesson et al. (2010) are also shown.

Table 4-5. Dry density after 2, 4, 6 and 11 years determined after dismantling of FLR5, FLR6, FLR7 and FLR8, respectively, and the corresponding total pressure measured on FLR2 with similar setup. (Data from FLR5, FLR6 and FLR7 see Dueck et al., (2018, 2022). See also Table 4-1

Time		2 years	4 years	6 years	11 years	2 years	4 years	6 years	11 years
Sample ID		FLR5	FLR6	FLR7	FLR8	FLR2 ⁶	FLR2 ⁶	FLR2 ⁶	FLR2 ⁶
Distance ¹	Pellet/block ²	Dry density				Total pressure			
mm		kg/m ³	kg/m ³	kg/m ³	kg/m ³	kPa	kPa	kPa	kPa
250	Pellet ³	946	950	987	1044	179	309	408	402
187.5	Pellet ⁴	1046	1047	1042	1038	247	232	242	266
62.5	Block ⁴	1476	1429	1399	1367	3381	3066	2235	2265
0	Block ³	1588	1581	1553	1480 ⁵	6231	5981	5440	5296

¹ Measured from the bottom. ² Initial type. ³ The total pressure was measured axially as load on a piston. ⁴ The total pressure was measured radially as load on a piston. ⁵ Uncertain value, see section 4.2. ⁶ FLR2 has similar setup as FLR5, FLR6, FLR7 and FLR8.

Table 4-6. Dry density after 11 years determined after dismantling of FLR3 and the corresponding total pressure. See also Table 4-1 and Table 4-5

Time		11 years	11 years
Sample ID		FLR3	FLR3
Distance ¹	Pellet/block ²	Dry density	Total pressure ⁵
mm		kg/m ³	kPa
250	Pellet ³	1021	412 ⁵
187.5	Pellet ⁴	1029	255
62.5	Block ⁴	1382	2249
0	Block ³	1440 ⁶	5430

¹ Measured from the bottom. ² Initial type. ³ The total pressure was measured axially as load on a piston.

⁴ The total pressure was measured radially as load on a piston. ⁵ The total pressure was evaluated after lowering the water pressure to zero, which only affected the axially measured stress on the pellet side, see Table 4-1. ⁶ Uncertain value, see section 4.2.

In the diagram of the stress evolution with time in Figure 4-1 and Figure 4-2 a decrease is observed in the axial stress measured from the bottom of the setup (blue markers). In March 2018 all devices in the FLR-series were moved to another laboratory facility and the average temperature increase approximately one degree. At that time FLR5 and FLR6 were already dismantled. The decrease observed in the axial stress is probably related to the expansion of the steel tubes, however small. Similar stress decrease in the lower block part of the setup was also observed in the other instrumented tests, see Appendix 1 where the measured swelling pressures are shown together with the temperature. See also Dueck et al. (2018, 2022).

A fluctuation of the stresses over a shorter time period was also observed. The fluctuation corresponded well to the fluctuation of the temperature but in this case an increase in temperature resulted in an increase in the measured stresses. The probable explanation for this is that an increase in temperature causes volume expansion of the water in the bentonite and with the geometry used, i.e. long tubes with drainage at one end only, it takes some time for the excess water pressure to disappear. This is illustrated in Appendix 1, where the measured stresses for 5 weeks (2024-05-25 to 2024-06-29) are shown together with the temperature. The higher and lower stresses are shown in separate diagrams to increase the resolution.

5 Investigation of the homogenisation process

The main goal of the study described in this chapter is to investigate the process of homogenisation in a long-term perspective. Can significant changes of the dry density distributions, towards a more homogeneous state, be seen in the data? The experiment provides data in form of dry density distributions when the tests are dismantled and (for some tests) measurements of axial and radial stresses during operation.

Two different approaches were used for analysing test data regarding homogenisation. A direct approach, investigating the properties of the obtained dry density distribution using statistics, and an indirect approach, where the friction between the bentonite and tube wall was evaluated using an analytical mechanical model, equipped with properties obtained from the test data set.

5.1 Direct approach – statistical method

Here, the standard deviation, s , of the dry density distributions was calculated for each terminated test (FLR5 (2 yr), FLR6 (4 yr), FLR7 (6 yr), FLR8 (11 yr), and FLR3 (11 yr)) and a new variable describing the “magnitude of homogenisation” was defined using s and the standard deviation for the initial state, s_0 .

The standard deviation and average value, $\bar{\rho}_d$, are given by,

$$s^2 = \frac{1}{H} \sum (\rho_d^i - \bar{\rho}_d)^2 \Delta y^i \quad (5-1)$$

$$\bar{\rho}_d = \frac{1}{H} \sum \rho_d^i \Delta y^i \quad (5-2)$$

where Δy^i denotes the sample height at $y = y^i$, $H = \sum \Delta y^i$ denotes the total length of the buffer, and ρ_d^i the determined dry density at $y = y^i$.

A new variable, $h = 1 - s/s_0$, was formulated by normalization of s using the standard deviation for the initial state s_0 . This results in $h = 0$ when $s = s_0$, i.e. for no homogenisation, and $h = 1$ when $s = 0$, i.e. for total homogenisation.

The results from performing the calculations are given in Table 5-1 and the evolution of the homogenisation indicator h and its rate, evaluated by $\Delta h/\Delta t$, is shown in Figure 5-1. The findings are:

- Homogenisation has progressed with time between all terminated tests.
- The rate of progression decreases with time, i.e. $\Delta h/\Delta t$ decreases with time.
- The remarkable agreement between the two last tests indicates, somewhat surprisingly, that homogenisation in the tests is independent of surface roughness.

It must be remembered that the dataset is very limited and that there are inaccuracies which could affect the result. One such issue is the disagreement between data reported at installation and at dismantling, discovered when performing the calculations. Below follows a discussion of the total solid mass obtained from using data from installation and dismantling. After this follows a description of how the disagreement in data was handled when performing the analysis.

Table 5-1. Data used for describing the homogenisation of the determined dry density distribution

	FLR5	FLR6	FLR7	FLR8	FLR3
Time [years]	2	4	6	11	11
$\bar{\rho}_d$ [kg/m ³]	1270	1251	1239	1217	1223
s_0 [kg/m ³]	278	297	305	323	327
s [kg/m ³]	231	205	192	165	170
h [-]	0.17	0.31	0.37	0.49	0.48
$\Delta h/\Delta t$ [1/y]	0.085	0.070	0.030	0.024	0.022

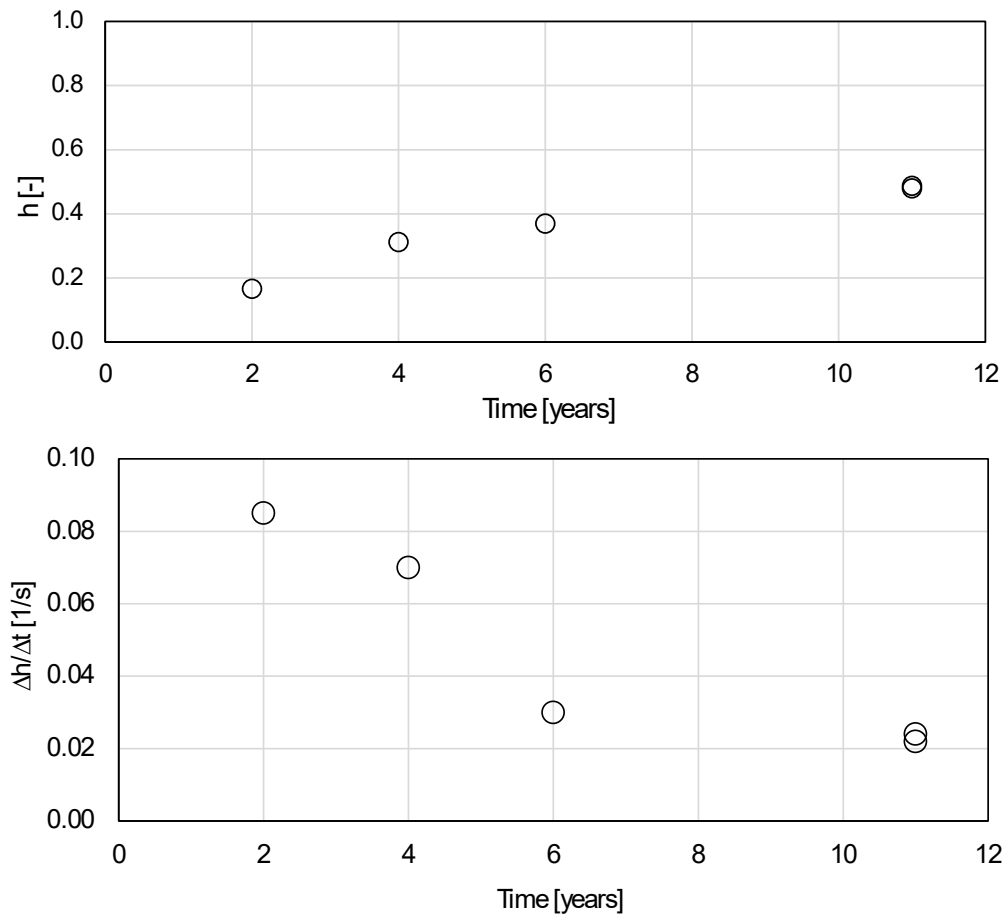


Figure 5-1. Time evolution of the homogenisation indicator h (top) and its rate $\Delta h/\Delta t$ (bottom).

5.1.1 Disagreement between data reported at installation and dismantling

When carrying out the study it became apparent that there was a disagreement between data at installation and dismantling. To investigate this further and finding a way to address this in the analysis, data regarding total solid mass was used.

Total solid mass at installation $m_s(t_0)$, at dismantling $m_s(t_{end})$, and from using the dry density distribution, $\sum \rho_d^i \Delta y^i$ are shown in Table 5-2. $m_s(t_{end})$ is, as expected, somewhat lower as compared to $m_s(t_0)$, some loss of material is expected during dismantling. The result from using the dry density distribution does, however, not agree very well with $m_s(t_{end})$, which is expected. For all tests $\sum \rho_d^i \Delta y^i > m_s(t_{end})$, and $\sum \rho_d^i \Delta y^i > m_s(t_0)$ for all tests except for FLR3 where $\sum \rho_d^i \Delta y^i = m_s(t_0)$.

From our understanding, this must come from an inaccuracy in the dry density distribution. The source could be in the translation between water content to dry density, $\rho_d = \rho_s / (1 + w\rho_s/\rho_w)$ assuming $S_t = 1$, or when measuring the sample position and height.

The uncertainty in the translation between w and ρ_d is considered to be insignificant. The determined degree of saturations has consistently showed full saturation. Solid and dry densities are well known, and w is calculated from mass measurements which have high accuracy. The inaccuracy is therefore most likely an effect from inaccuracies in measurements of sample heights and sample positions.

Table 5-2. Compilation of total solid mass

	FLR3	FLR5	FLR6	FLR7	FLR8
$m_s(t_0)$ [kg]	0.149	0.160	0.161	0.160	0.161
$m_s(t_{end})$ [kg]	0.146	0.144	0.150	0.143	0.158
$\sum \rho_d^i \Delta y^i$ [kg]	0.149	0.170	0.166	0.166	0.163

Returning to the analysis, the disagreement was seen when calculating s_0 , which is obtained by,

$$s_0^2 = \frac{1}{H} \left((\rho_d^b - \bar{\rho}_d(t_0))^2 H_b + (\rho_d^p - \bar{\rho}_d(t_0))^2 H_p \right), \quad (5-3)$$

where ρ_d^b denotes the initial dry density (after radial swelling) for the block section, ρ_d^p the initial dry density for the pellet section, and H_b and H_p their heights, respectively. Ideally, all ingoing quantities will be known from the initial state of the experiment, but for the study reported here there are some complications due to some disagreement between data described above.

To address the discrepancy, the measurements at the end of the test are assumed to be correct and an assumption of no loss of solid mass during the operational phase is made, $\bar{\rho}_d(t_0) = \bar{\rho}_d$. To get an initial state in agreement with the determined density distribution at the end of the test, the following relation in terms of dry densities and heights can be used,

$$(H_b + H_p) \bar{\rho}_d = H_b \rho_d^b + H_p \rho_d^p. \quad (5-4)$$

Besides the average dry density, the block section's initial dry density, ρ_d^b , and initial height, H_b , are known. The initial dry density of the pellet section, ρ_d^p , can be expressed in terms of the installed bentonite pellets mass, m_p , the initial water content, w_p , and the initial volume, $\pi r^2 H_p$, according to:

$$\rho_d^p = \frac{1}{\pi r^2 H_p} \frac{m_p}{w_p + 1}. \quad (5-5)$$

In the two Equations 5-4 and 5-5, ρ_d^p and H_p are the only unknowns which therefore can be solved for. This enables calculation of s_0 , according to (5-3), in agreement with the measured dry density distributions. The initial data for the tests can be found in Table 6-2 in the report by Dueck et al. (2018). Table 5-3 shows the obtained values for H_p , ρ_d^p , and s_0 . It should be noted that there is a disagreement between the total length H measured at dismantling, used when calculating $\bar{\rho}_d$ and s , and that obtained by $H_b + H_p$, used when calculating s_0 . The discrepancy ($H_b + H_p - H$) is also shown in Table 5-3 to indicate the “accuracy” of the different tests. This information is valuable to have in mind at future dismantling.

Table 5-3. Parameters in agreement with the measured dry density distributions

	FLR5	FLR6	FLR7	FLR8	FLR3
H_p [m]	0.113	0.117	0.119	0.124	0.123
$H_b + H_p - H$ [mm]	-14.3	-8.2	-8.7	-3.0	-0.4
ρ_d^p [kg/m ³]	978	944	926	892	894
s_0 [kg/m ³]	278	297	305	323	327

5.2 Indirect approach – analytical mechanical representation

The distribution of bentonite along the tube can be analysed indirectly evaluating a friction angle, ϕ , from an analytical model previously used and presented in Dueck et al. (2019) which is described by Equations 5-6 and 5-7.

In short, the model is based on the force equilibrium of a thin circular disc, with radius r , of buffer subjected to an axial stress σ_a and a friction induced shear stress $\tau = \sigma_n \tan \phi$, acting on the outer surface with the normal stress, σ_n . It was then assumed that $\sigma_n = \sigma_a$ which enabled variable separation and integration of the differential equation from $z = z_0$, where $\sigma_a(z_0) = \sigma_0$, to $z = z_0 + \Delta z$, where $\sigma_a(z_0 + \Delta z) = \sigma$. This resulted in,

$$\ln\left(\frac{\sigma}{\sigma_0}\right) = -\frac{2 \Delta z \tan \phi}{r}. \quad (5-6)$$

Where available, sensor positions, z_0 and $z_0 + \Delta z$, and corresponding stress measurements, σ_0 and σ , can be used directly in Equation 5-6 to obtain an estimate of the friction angle. Table 5-4 shows the friction angles obtained for FLR2 and FLR3 when calculated using the given radial stress measurements averaged over the latest two-year period together with the indicated average inner tube radius, r and $\Delta z = 0.125$ m.

Table 5-4. Friction angles obtained from using stress measurements

	FLR2	FLR3
σ_0 [MPa]	2.22	2.37
σ [MPa]	0.272	0.318
$2r$ [m]	0.025	0.026
ϕ [deg]	6.2	5.7

Another method uses the determined dry density distribution together with a swelling pressure curve, $p_s = f(\rho_d)$. Equation 5-7 is an example of such a swelling pressure curve, taken from Börjesson et al. (1995). Other expressions representing a swelling pressure curve could of course be used, the reason behind this choice is to enable comparisons with existing analyses.

$$p_s = p_{s0} \cdot \left(\frac{e}{e_0}\right)^{1/\beta} \quad (5-7)$$

If using $\sigma = p_s$ and $\rho_d = \rho_s / (1 + e)$, providing the connection between void ratio e and dry density, Equation 5-7 gives input to Equation 5-6. In Equation 5-7 the used reference values are $p_{s0} = 1$ MPa and $e_0 = 1.1$, and β is given different values depending on the value of dry density,

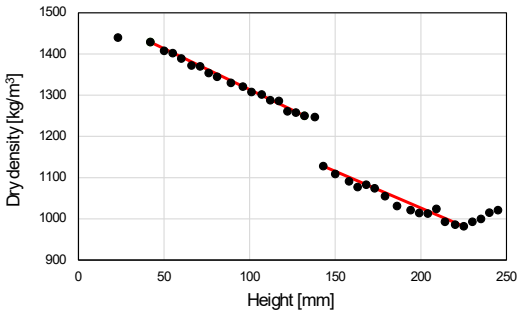
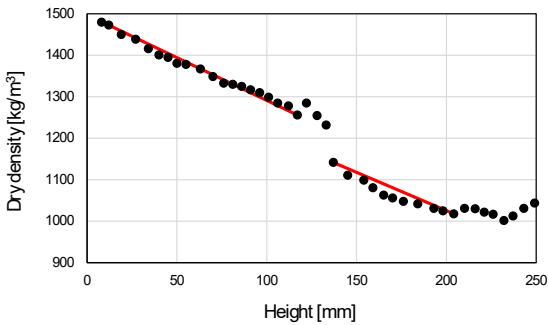
$$\beta = \begin{cases} -0.19 & \text{for } \rho_d \geq 1200 \text{ kg/m}^3 \\ -0.23 & \text{for } \rho_d < 1200 \text{ kg/m}^3 \end{cases} \quad (5-8)$$

see test results presented by e.g. Börjesson et al. (1995).

As the dry density distributions have such clear separation at the interface between the block and pellet section, see graphs in Table 5-5, the friction angle evaluation was first made separately for the block and pellet section. In the graphs in Table 5-5 the endpoints of the red lines indicate the input data for the analytical model. The result from the evaluation is shown below the graphs in Table 5-5. To facilitate comparisons with existing friction angle evaluations, “overall” friction angles were also calculated using the bottom and top endpoint data in the block and pellet filled section, respectively. The result is shown at the bottom in Table 5-5.

It should be noted that the analysis of friction angles is based on some assumptions. One is that the stress state always is isotropic, i.e. that the axial and radial stress components are always equal in all points. In tests where the two stress components are measured during axial loading/unloading in an oedometer, the components generally disagree. Another assumption is made when the swelling pressure curve is selected. Experiments show that the initial state of the material before installation as well as the hydromechanical process it undergoes (wetting/drying/swelling/compaction) determine the so-called swelling pressure curve. There is also some uncertainty using Equation 5-7 for both buffer sections over the active range in dry density (void ratio) and the different hydromechanical conditions. Based on some tentative comparisons against small scale experiments, the representation seems reasonable for the compacted block section. Using this representation for the pellet filling is more questionable, much so due to the significant compression of this part.

Table 5-5. Input to calculation of friction angles in block and pellet slot sections

FLR3		FLR8	
			
Block section: $\phi = 5.4^\circ$ Pellet section: $\phi = 4.2^\circ$		Block section: $\phi = 5.8^\circ$ Pellet section: $\phi = 4.5^\circ$	
Overall: $\phi = 5.9^\circ$		Overall: $\phi = 6.0^\circ$	

6 Concluding remarks

The study presented is belonging to a research topic where the homogenisation properties of bentonite are studied with long-time homogenisation tests in steel tubes. The purpose of these tests is to study the effect of friction for limiting homogenisation and also to study the influence of time on the remaining density gradients after completed swelling and compression.

Initially, ten tests of this type were started, and MX-80 was used for all specimens. Five of the specimens have been dismantled and the results of two of the dismantled specimens, dismantled after 11 years, have been reported here. The results have been presented in terms of dry density distributions and stress measurements. The new data is also compared to what was obtained for the previously completed tests.

The long-term perspective of the homogenisation process in the tests was studied using two different approaches. In a direct approach, a homogenisation indicator was formulated using statistical properties of the dry density distribution. An indirect approach, used previously in the research topic, is based on an analytical solution of a mechanical model which includes friction between the buffer and the tube inner surface. The outcome from this is an estimate of a friction angle.

The findings from the direct approach are (see Figure 5-1):

- The homogenisation is progressing at a decreasing rate.
- There is a remarkable agreement between the two last tests in terms of progression in homogenisation. This indicates that homogenisation in the tests is independent of surface roughness.

The findings from the indirect approach also agrees well with the list above. The computed friction angles agree well with values computed in earlier analyses.

When performing the analysis, it became clear that there was an inaccuracy in the dry density distribution which results in an overestimation of the solid mass. The inaccuracy is most likely an effect from inaccuracies in measurements of sample heights and sample positions.

References

SKB's (Svensk Kärnbränslehantering AB) publications can be found at www.skb.com/publications.

Börgesson L, Johannesson L-E, Sandén T, Hernelind J, 1995. Modelling of the physical behaviour of water saturated clay barriers. Laboratory tests, material models and finite element application. SKB TR 95-20, Svensk Kärnbränslehantering AB.

Dueck A, Börgesson L, 2021. Bentonite homogenisation. Three studies based on laboratory tests results. SKB P-21-05, Svensk Kärnbränslehantering AB.

Dueck A, Goudarzi R, Börgesson L, 2018. Buffer homogenisation - status report 4. SKB TR-17-04, Svensk Kärnbränslehantering AB.

Dueck A, Börgesson L, Kristensson O, Malmberg D, Åkesson M, Hernelind J, 2019. Bentonite homogenisation. Laboratory study, model development and modelling of homogenisation processes. SKB TR-19-11, Svensk Kärnbränslehantering AB.

Dueck A, Goudarzi R, Jensen V, Börgesson L, 2022. Buffer homogenisation - status report 5. SKB TR-21-14, Svensk Kärnbränslehantering AB.

Karnland O, Olsson S, Nilsson U, 2006. Mineralogy and sealing properties of various bentonites and smectite-rich clay materials. SKB TR-06-30, Svensk Kärnbränslehantering AB.

Svensson D, Dueck A, Nilsson U, Olsson S, Sandén T, Lydmark S, Jägerwall S, Pedersen K, Hansen S, 2011. Alternative buffer material. Status of the ongoing laboratory investigation of reference materials and test package 1. SKB TR-11-06, Svensk Kärnbränslehantering AB.

Åkesson M, Börgesson L, Kristensson O, 2010. SR-Site Data report. THM modelling of buffer, backfill and other system components. SKB TR-10-44, Svensk Kärnbränslehantering AB.

Appendix 1

Results from the FLR-series

Below the evolution of total stress from the setups FLR1 to FLR4 are shown. The setups are shown in Figure 3-1 Figure 3-2. The total stress (including the water pressure of 70 kPa) is measured as a load on a piston with the diameter 25 or 35 mm in case of axial measurements and 10 mm in case of radial measurements.

Below the evolution of total stress from the instrumented setups FLR1-FLR4 are shown (Figure A1-1 to Figure A1-2) from start and until 2024-06-27. The evolutions during the last 5 weeks are then shown in higher resolution (Figure A1-3 to Figure A1-6). The timetables of the dismantled FLR3 and FLR8 are shown in Table A1-1 and Table A1-2. In Table A1-3 and Table A1-4 the distributions of water content and dry density of the dismantled FLR3 and FLR8 are shown. Finally, the status of the initially 10 steel tubes are shown in Table A1-5.

The setup FLR3 was dismantled 2024-06-27. Nine days before dismantling the water pressure of 70 was adjusted to zero. This can be seen in the evolution of the axial stress on the pellets side of FLR3 to the right in Figure A1-5 (light blue markers). After the dismantling the load cells used for the evaluation of stresses were checked. The error of the load cells used for the measurements in the lower part, i.e. the block part with higher stresses, showed an error less than 7 %. However, the load cells used for the upper pellet part with low stress levels showed error of -27 % to -40 %. This means that the stress measured radially at the pellet side of FLR3 $P=255$ kPa and the stress measured axially at the pellet side of FLR3 $P=412$ kPa was higher and approximately 350 kPa and 687 kPa, respectively, cf Figure 3-2 Figure 4-5. However, in this report these errors are only noted and not used for any corrections of the stresses given in diagrams or tables.

Total stress evolution of FLR1 – 4

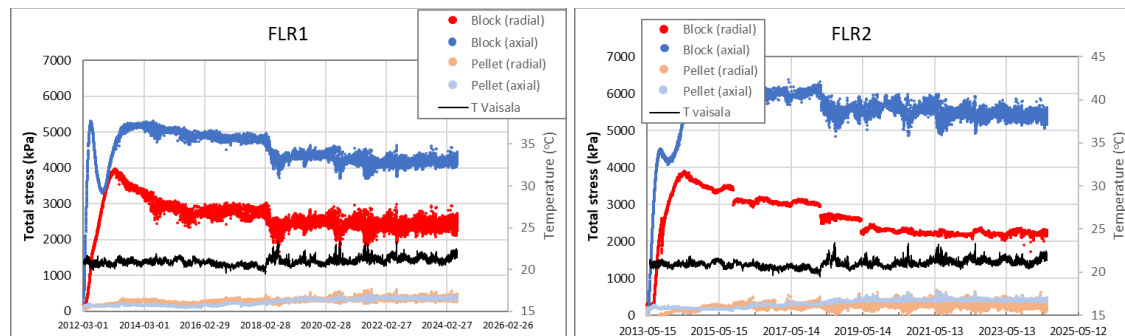


Figure A1-1. Total stress evolution until 2024-06-27 from setup FLR1(to the left) and FLR2 (to the right). The setup FLR2 resembles that of FLR5-FLR10.

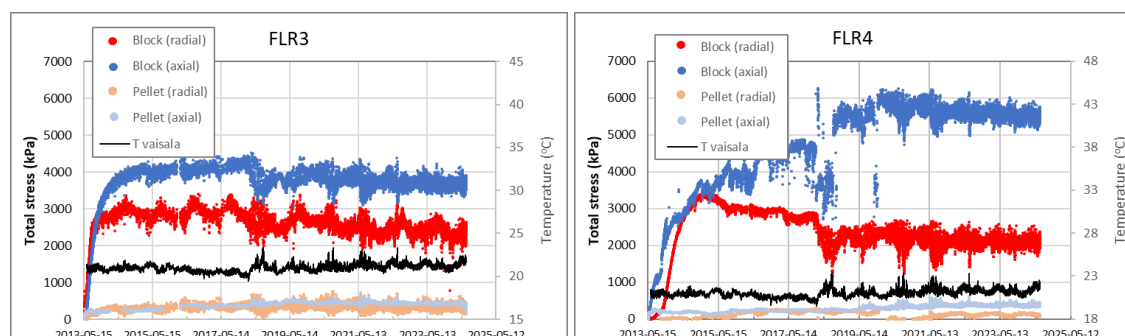


Figure A1-2. Total stress evolution until 2024-06-27 from setup FLR3 (to the left) and FLR4 (to the right). The setup FLR3 was dismantled on 2024-06-27.

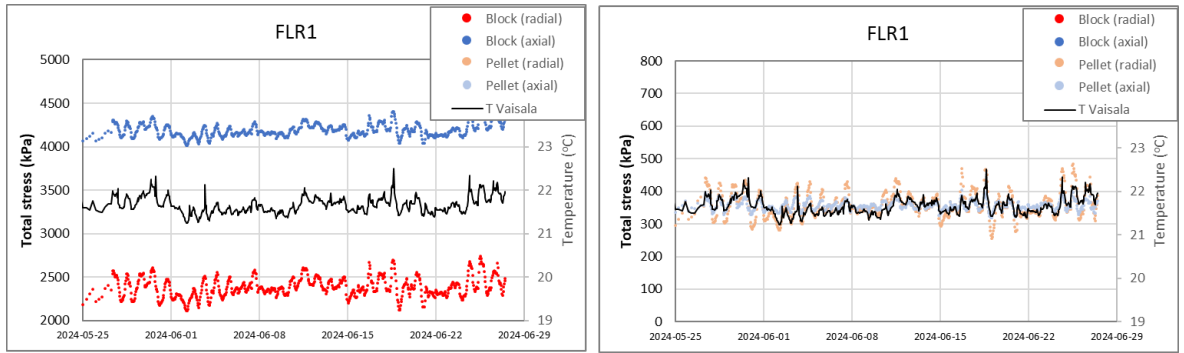


Figure A1-3. Illustration of the influence of temperature. Total stress evolution from setup FLR1 between 2024-05-25 to 2024-06-29 with measurements from the lower block part (to the left) and from the upper pellet part (to the right) in separate diagrams.

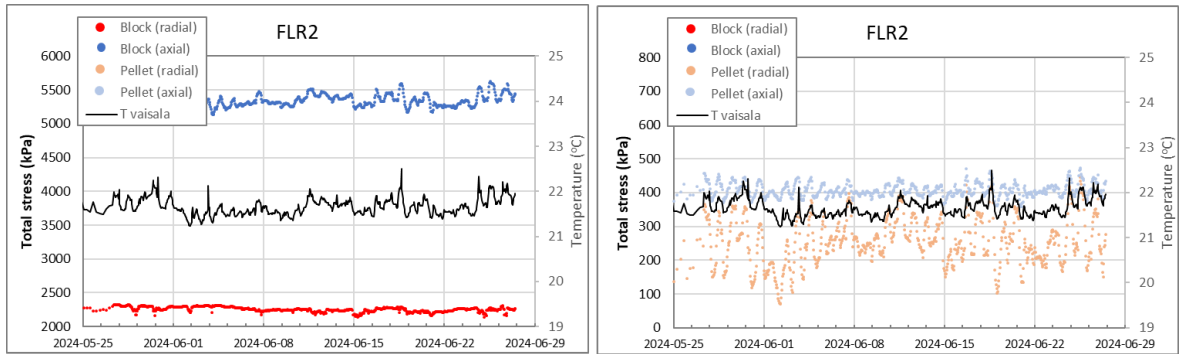


Figure A1-4. Illustration of the influence of temperature. Total stress evolution from setup FLR2. See Figure A1-3.

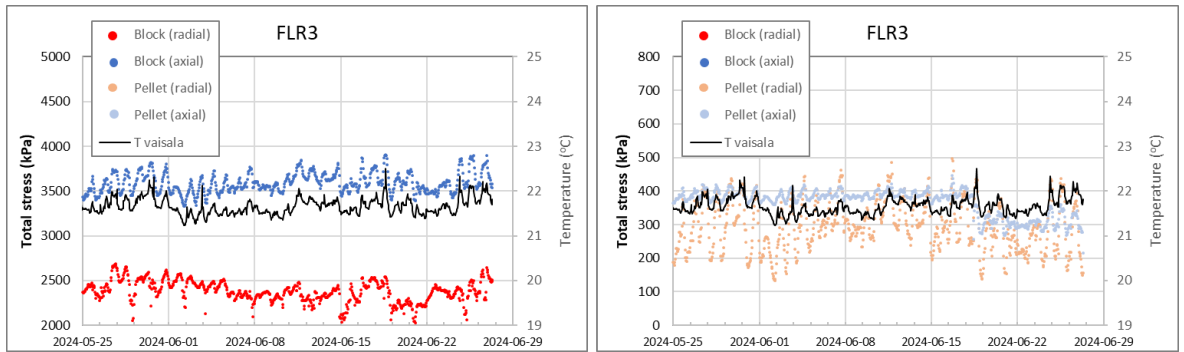


Figure A1-5. Illustration of the influence of temperature. Total stress evolution from setup FLR3. See Figure A1-3. On 2024-06-18 the water pressure was lowered on set-up FLR3, from the stresses this was only seen in the axial stress from the pellet side (light blue marker). FLR3 was dismantled on 2024-06-27, see also Table A1-1.

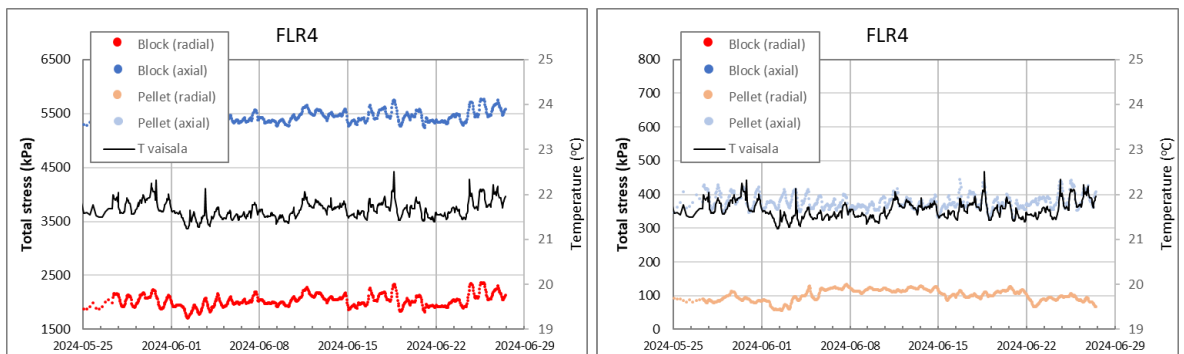


Figure A1-6. Illustration of the influence of temperature. Total stress evolution from setup FLR4. See Figure A1-3.

Timetables of FLR3 and FLR8

Table A1-1. Timetable from start to end of FLR3

Study	Buffer homogenisation	
	Long steel tubes	
Test ID	FLR-3	
Information	Sensors	Yes
	Equipment	Steel cylinder with triangular grooves along the inner surface
	Sensors	Four load cells, two located axially and two located radially
	Material	MX-80 five compacted blocks, lower part
		MX-80 extruded pellet, upper part
	Water	2 mM NaCl at first but later changed to 50 mM NaCl
Date/time	Comments	
2013-05-22	Test start	
2013-05-22	Device assembled and specimen mounted	
2013-05-22	Water added (vacuum used)	
2013-05-22	Water circulation through the filter was made appr. once a week	
2013-08-07	Water circulation through the filter was made appr. once a month until 2020-11-03	
2015-10-05	Continuous water pressure of 70 kPa applied	
2016-03-03	Problems with sensor measuring axial stress in pellet	
2016-05-10	Problem with sensor has been corrected	
2018-03-05	Moving test devices to new facility	
2018-08-09	Recurring problem with power supply and acquisition system	
2018-11-29	Problems with power supply and data acquisition fixed	
2019-06-07	Problem with power supply and acquisition system	
2019-07-31	Recurring problem with power supply and acquisition system	
2020-01-13	Problems with power supply and data acquisition fixed	
2020-11-03	Flushing at least every 4th month	
2024-06-18	Water pressure adjusted to zero	
2024-06-27	End of test and dismantling	

Table A1-2. Timetable from start to end of FLR8

Study	Buffer homogenisation	
	Long steel tubes	
Test ID	FLR-8	
Information	No sensors	
	Equipment	Steel cylinder with triangular grooves along the inner surface
	Sensors	No
	Material	MX-80 five compacted blocks, lower part
		MX-80 extruded pellet, upper part
	Water	2 mM NaCl at first but later changed to 50 mM NaCl
Date/time	Comments	
2013-05-17	Test start	
2013-05-17	Device assembled and specimen mounted	
2013-05-17	Water added (vacuum used)	
2013-05-17	Circulation of water	
	Water circulation through the filter was made appr. once a week	
2013-08-07		
	Water circulation through the filter was made appr. once a month	
2015-10-05	Continuous water pressure of 70 kPa applied	
	Flushing approximately once a month	
2018-03-05	Moving test devices to new facility	
	Flushing approximately once a month	
2020-11-03		
	Flushing approximately every 4th month	
2024-06-04	Water pressure adjusted to zero	
2024-06-07	End of test and dismantling	

Distribution of water content after dismantling

Table A1-3. Distribution of water content after dismantling of FLR3. The dry density is calculated from a measured water content and a degree of saturation $S_r = 100$ %. At five positions the dry density is also calculated, from measured water content and measured bulk density

FLR3 Sample ID	Thickness mm	Distance ¹ mm	Water content %	Dry density (from bulk density) kg/m ³	Dry density (assume $S_r=100$ %) kg/m ³
1	5.15	245	61.9		1021
2	5.15	240	62.6		1015
3	5.15	235	64.0		1000
4	5.15	230	64.7		993
5	5.15	225	65.9		982
6	5.15	220	65.4		986
7	5.15	214	64.8		993
8	5.15	209	61.7		1024
9	5.15	204	62.8		1013
10	5.15	199	62.6		1014
11	5.15	194	62.0		1021
12	10.15	186	61.0	1038	1031
13	5.15	179	58.8		1055
14	5.15	173	57.2		1074
15	5.15	168	56.4		1083
16	5.15	163	56.9		1077
17	5.15	158	55.7		1091
18	10.15	150	54.2	1114	1109
19	5.15	143	52.7		1128
20	5.15	138	44.2		1247
21	5.15	132	44.0		1250
22	5.15	127	43.5		1258
23	5.15	122	43.3		1261
24	5.15	117	41.8		1286
25	5.15	112	41.7		1288
26	5.15	107	40.8		1302
27	5.15	101	40.5		1308
28	5.15	96	39.7		1321
29	10.15	89	39.2	1335	1330
30	5.15	81	38.4		1345
31	5.15	76	37.9		1354
32	5.15	71	37.0		1370
33	5.15	66	36.9		1372
34	5.15	60	36.0		1389
35	5.15	55	35.4		1402
36	5.15	50	35.0		1408
37	10.15	42	34.0	1434	1429
38	38.08 ²	23			1440 ³

¹ Distance from the bottom to centre of the sample. ² Uncertain position of the lower 38 mm. ³ Average value.

Table A1-4. Distribution of water content after dismantling of FLR8. The dry density is calculated from a measured water content and a degree of saturation $S_r = 100$ %. At five positions the dry density is also calculated, from measured water content and measured bulk density

FLR8 Sample ID	Thickness	Distance ¹	Water content	Dry density (from bulk density)	Dry density (assume $S_r=100$ %)
	mm	mm	%	kg/m ³	kg/m ³
1	5.15	249	59.8		1044
2	7.15	243	61.0		1031
3	5.15	237	62.8		1013
4	5.15	232	63.8		1002
5	5.15	226	62.3		1017
6	5.15	221	61.9		1022
7	5.15	216	61.1		1030
8	6.15	210	61.0		1031
9	6.15	204	62.2		1018
10	6.15	198	61.6		1025
11	5.15	193	61.1		1031
12	11.15	184	60.0	1050	1042
13	5.65	176	59.4		1048
14	5.65	170	58.7		1056
15	5.65	165	58.1		1063
16	5.15	159	56.5		1081
17	5.15	154	55.0		1099
18	12.15	145	54.0	1121	1111
19	4.15	137	51.6		1142
20	4.65	133	45.2		1232
21	5.65	128	43.7		1255
22	5.65	122	41.9		1285
30	5.15	117	43.6		1256
31	5.15	112	42.3		1278
32	5.15	106	41.8		1285
33	5.15	101	41.0		1299
34	5.15	96	40.4		1310
35	5.15	91	40.0		1317
36	5.15	86	39.5		1325
37	5.15	81	39.2		1330
38	5.15	76	39.0		1333
39	5.15	70	38.2		1349
40	10.15	63	37.2	1372	1367
41	5.15	55	36.6		1378
42	5.15	50	36.4		1381
43	5.15	45	35.7		1395
44	5.15	40	35.4		1401
45	5.15	34	34.7		1416
46	10.15	27	33.5	1447	1439
47	5.15	19	33.0		1450
48	10.15	12	31.9	1486	1473
49	6.45 ²	8			1480 ³

¹ Distance from the bottom to centre of the sample. ² Uncertain position of the lower 6 mm. ³ Average value.

Status of FLR1-10

Table A1-5. Status of the ten installed stell tubes FLR1 – FLR10

Friction Long Tube (FLR)										
Labels	FLR1	FLR2	FLR3	FLR4	FLR5	FLR6	FLR7	FLR8	FLR9	FLR10
Start date	2012-03-09	2013-05-15	2013-05-22	2013-05-23	2013-05-15	2013-05-16	2013-05-16	2013-05-17	2013-05-17	2013-05-20
End of test			2023-06-27		2015-05-20	2017-05-29	2019-05-02	2024-06-07		
Set-up										
Total height (mm)	250			350	250					
Final average diameter (mm)	26	26	25	36	26					
Inside friction (grooves)	rectangular	triangular	smooth	triangular	triangular	triangular	triangular	triangular	triangular	triangular
Transducers	yes				no					
Material upper half	MX-80 pellet (extruded)									
Material lower half	MX-80 buffer									
Water supply	only from the pellet side and initially added by circulation									
Type of water	0.2 mM/2 mM/50 mM NaCl									
Target final dry density										
Upper part $\rho_{d,upper}$ (kg/m ³)	772	882	882	882	882	882	882	882	882	882
Lower part $\rho_{d,lower}$ (kg/m ³)	1566	1561	1561	1561	1561	1561	1561	1561	1561	1561